

Metal-Organic Frameworks

How to cite:

International Edition: doi.org/10.1002/anie.202217377

German Edition: doi.org/10.1002/ange.202217377

Twisting of Porphyrin by Assembly in a Metal-Organic Framework yielding Chiral Photoconducting Films for Circularly-Polarized-Light Detection

Chun Li, Henrik Schopmans, Lukas Langer, Stefan Marschner, Abhinav Chandresh, Jochen Bürck, Youichi Tsuchiya, Adachi Chihaya, Wolfgang Wenzel, Stefan Bräse, Mariana Kozłowska,* and Lars Heinke*

Abstract: While materials based on organic molecules usually have either superior optoelectronic or superior chiral properties, the combination of both is scarce. Here, a crystalline chiroptical film based on porphyrin with homochiral side groups is presented. While the dissolved molecule has a planar, thus, achiral porphyrin core, upon assembly in a metal-organic framework (MOF) film, the porphyrin core is twisted and chiral. The close packing and the crystalline order of the porphyrin cores in the MOF film also results in excellent optoelectronic properties. By exciting the Soret band of porphyrin, efficient photoconduction with a high On-Off-ratio is realized. More important, handedness-dependent circularly-polarized-light photoconduction with a dissymmetry factor g of 4.3×10^{-4} is obtained. We foresee the combination of such assembly-induced chirality with the rich porphyrin chemistry will enable a plethora of organic materials with exceptional chiral and optoelectronic properties.

Introduction

Photonics based on circularly polarized light (CPL) is intensively explored for applications in quantum optics, quantum computing, information processing and remote sensing.^[1] For these purposes, the material must show chiral optoelectronic properties, which results in different excitations when absorbing photons of left-handed CPL (LCP) or right-handed CPL (RCP). Ideally, such materials combine both high chiroptical response and efficient charge transport simultaneously.^[2] In the context of different applications, like printed electronics, light-emissive devices or photo-

voltaics as well as in the context of stretchable electronics and photosensors, semiconducting organic materials feature striking advantages over inorganic materials.^[3] Porphyrin-based materials are among the materials which attract particular attention for organic-semiconductor light-harvesting applications like in photovoltaic devices and for photocatalysis.^[4] Porphyrin molecules are excellent electron donor molecules with delocalized planar π -systems.^[5] In the visible light range, porphyrins exhibit sharp and intensive absorption bands, perfectly suited for applications in light harvesting.^[4c] To this end, porphyrins are often integrated as active components in various optoelectronic devices.^[6]

[*] C. Li, A. Chandresh, Dr. L. Heinke
 Karlsruhe Institute of Technology (KIT), Institute of Functional Interfaces (IFG)
 Hermann-von-Helmholtz-Platz 1, 76344 Eggenstein-Leopoldshafen (Germany)
 E-mail: Lars.Heinke@kit.edu

H. Schopmans, Prof. Dr. W. Wenzel, Dr. M. Kozłowska
 Karlsruhe Institute of Technology (KIT), Institute of Nanotechnology (INT)
 Hermann-von-Helmholtz-Platz 1, 76344 Eggenstein-Leopoldshafen (Germany)
 E-mail: Mariana.Kozłowska@kit.edu

L. Langer, S. Marschner, Prof. Dr. S. Bräse
 Karlsruhe Institute of Technology (KIT), Institute of Organic Chemistry (IOC)
 Fritz-Haber-Weg 6, 76131 Karlsruhe (Germany)

Dr. J. Bürck
 Karlsruhe Institute of Technology (KIT), Institute of Biological Interfaces (IBG-2)
 Hermann-von-Helmholtz-Platz 1, 76344 Eggenstein-Leopoldshafen (Germany)

Dr. Y. Tsuchiya, Prof. A. Chihaya
 Center for Organic Photonics and Electronics Research (OPEA), Kyushu University
 744 Motooka, Nishi-ku, Fukuoka 819-0395 (Japan)

Prof. A. Chihaya
 International Institute for Carbon Neutral Energy Research (WPI-I2CNER), Kyushu University
 744 Motooka, Nishi-ku, Fukuoka 819-0395 (Japan)

Prof. Dr. S. Bräse
 Karlsruhe Institute of Technology (KIT), Institute of Biological and Chemical Systems-Functional Molecular Systems (IBCS-FMS)
 Herman-von-Helmholtz-Platz 1, 76344 Karlsruhe (Germany)

© 2022 The Authors. Angewandte Chemie International Edition published by Wiley-VCH GmbH. This is an open access article under the terms of the Creative Commons Attribution Non-Commercial License, which permits use, distribution and reproduction in any medium, provided the original work is properly cited and is not used for commercial purposes.

Moreover, the optoelectronic properties of porphyrins can be tailored by various methods of organic chemistry, e.g. by adding electron-poor or electron-rich groups.^[7] While the core moiety of porphyrin is planar and achiral, various efforts have been undertaken to realize porphyrin-based materials with chiral properties. For example, functionalizing porphyrin with chiral side groups allows the realization of enantioselective catalytic reactions.^[8] By embedment of porphyrin in homochiral cyclodextrin, chiral host-guest complexes can be made.^[9] Chiral supramolecular assemblies of molecules with planar, achiral porphyrin moieties functionalized with chiral side groups were also realized.^[10] By covalently bonding molecules like binaphthyl to the porphyrin core at two opposite positions, these molecules are strapped around the porphyrin core, causing the porphyrin moiety to be distorted.^[11] This results in chiroptical properties of the molecules in solution, however, a crystalline assembly of such compounds is hindered by the “strap”. To date, solid materials made from such compounds with chiral optoelectronic properties have not yet been presented. Other chiral porphyrin-based optoelectronic materials have also not yet been presented.

Metal-organic frameworks (MOFs) are crystalline hybrid materials composed of metal nodes connected by organic linker molecules.^[12] In recent years, in addition to applications in gas loading and separation,^[13] MOFs have been widely used in optoelectronic applications.^[14] The key advantage of MOFs is their crystalline order with structural and functional tunability. MOFs can be altered by various pre- and post-synthetic methods. By preparing MOF films on an appropriate substrate in a layer-by-layer fashion, surface-mounted MOF (SURMOF) films with controlled thickness can be realized.^[15] The incorporation of chiral linker molecules in SURMOFs results in chiral nanoporous films with enantioselective properties, e.g. in adsorption.^[16] SURMOFs based on porphyrin enable the realization of photoconducting thin films with large on/off-ratios.^[17] There, the brilliant photoconduction properties are a result of the optoelectronic properties of porphyrin in the regular crystalline lattice of the SURMOF, allowing efficient charge transfer, which can be even enhanced by combining the assembly with acceptor molecules. Due to the structural planarity and the pristine achiral properties of porphyrin (and other optoelectronically active molecules commonly used in MOFs), photoconducting chiral MOF films responsive to CPL have not yet been presented to date.

In comparison to conventional chiral optoelectronic materials,^[18] MOFs, as a hybrid material,^[12] may advantageously combine the properties of organic and inorganic materials. MOFs are crystalline enabling the precise comparison with theoretical models. The tunability of MOFs allows the rational design of the crystal structure and material properties to a wide extent. The organic components of MOFs can be varied by additional groups, allowing a further tuning of the material properties without altering the scaffold structure. In addition, the straightforward MOF synthesis and the option to prepare the material in the form of defined thin films^[15] as well as heterostructures^[19] with

well-defined interfaces^[20] are advantages of this material class.

Here, we present a crystalline, chiral assembly of porphyrin and explore its photophysical properties. The porphyrin molecules are functionalized by dicarboxylic acid and by homochiral BINOL-moieties (Figure 1a). The porphyrin moiety exhibits a planar form when dissolved in different solvents. By assembling with zinc acetate to crystalline and oriented SURMOFs, the molecules are twisted and the porphyrin moiety becomes chiral. Insights in the molecular structure and its chiroptical response are provided by density-functional theory (DFT) and time-dependent DFT calculations combined with circular dichroism (CD) and UV/Vis spectroscopy. The chiral porphyrin-SURMOF shows photoconducting properties with a large On-Off ratio and a dissymmetry factor between right and left CPL of 4.3×10^{-4} when exciting the Soret band with 450 nm, demonstrating its function as CPL photodetector.

Results and Discussion

The employed porphyrin molecule, which is functionalized with *R*-BINOL side groups and dicarboxylic acid, is shown

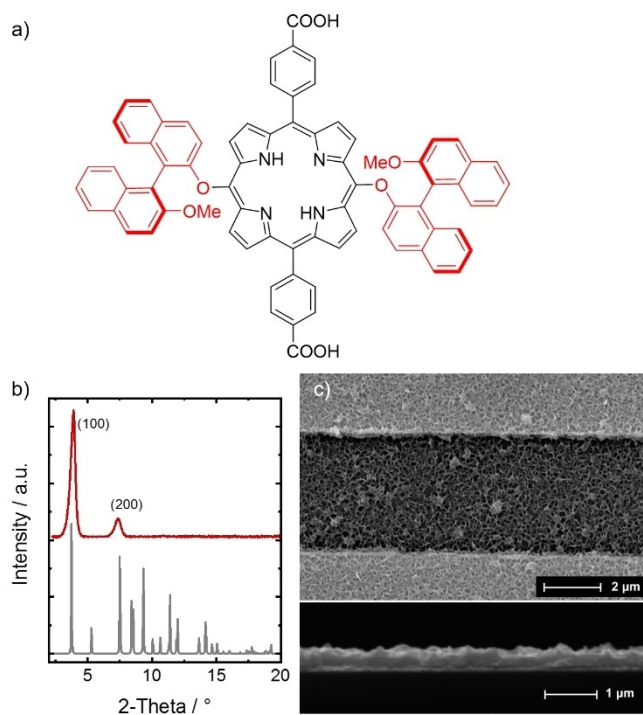


Figure 1. a) Molecular structure of *R*-MeBINOL-PorDC. The chiral *R*-BINOL-side groups are drawn in red, while the porphyrin core and the dicarboxylic acid side groups are in black. b) X-ray diffractogram of Zn(*R*-MeBINOL-PorDC) SURMOF. The red data are recorded for the sample, the grey data are calculated for the targeted structure. The experimentally observed reflexes are labelled. The X-ray wavelength is 0.154 nm. c) SEM images of Zn(*R*-MeBINOL-PorDC) SURMOF. The top-view is shown above, the side view of a broken sample is shown below. The sample is grown on quartz substrates with interdigitated gold electrodes, which are visible as bright stripes.

in Figure 1a. The molecule is referred to as *R*-MeBINOL-PorDC (4,4'-(10,20-bis(((*R*)-2'-methoxy-[1,1'-binaphthalen]-2-yl)oxy) porphyrin-5,15-diyl) dibenzoic acid). The synthesis is described in the Supporting Information. The molecule exhibits a planar structure of the porphyrin moiety with pendant non-planar and chiral *R*-BINOL moieties. The porphyrin molecule with the dicarboxylic acids in the para positions serves as linker molecule for the synthesis of MOF films. Together with zinc-paddle-wheels as metal nodes, MOF films with a SURMOF-2^[21] structure were prepared in a layer-by-layer fashion. The substrates are either quartz sheets (for UV/Vis and CD spectroscopy and atomic force microscopy), glass sheets with deposited interdigitated gold electrodes (for the conduction measurements as well as scanning electron microscopy and X-ray diffraction) or gold-coated silicon wafers (for infrared-reflection-absorption spectroscopy and energy-dispersive X-ray spectroscopy). The structure of the SURMOF film is referred to as Zn(*R*-MeBINOL-PorDC) SURMOF.^[22] The X-ray diffractogram (XRD) of the thin film shows a high crystallinity, Figure 1b. Moreover, the XRD shows that the film is grown in an oriented fashion with the (100) orientation perpendicular to the substrate surface.

The morphology of the thin film is explored by scanning electron microscopy (SEM), Figure 1c. The SEM images show that the film is homogeneous with a thickness of approximately 0.3 μm . They also show that the surface of the SURMOF possesses sheet-like crystallites on top, typical for films with a porphyrin-SURMOF-2-like structure.^[23]

The sample was further characterized by infrared-reflection-absorption spectroscopy (IRRAS) and energy-dispersive X-ray (EDX) spectroscopy and mapping, Figures S18–S20. The data from both techniques verify that the sample has the composition of the targeted Zn(*R*-MeBINOL-PorDC) structure. Imaging the sample surface with atomic force microscopy (AFM, Figure S21) shows that the MOF film has a roughness of approximately 72 nm and it verifies the thickness of about 300 nm (as also found by SEM).

The optical properties of the SURMOF are experimentally investigated by UV/Vis spectroscopy, Figure 2a. The spectrum of the SURMOF is compared with the spectrum of the linker in ethanolic solutions. Spectra of the linker in different solvents are shown in Figure S1a. Since the zinc-paddle-wheel-node has no significant electronic excitations in the UV/Vis range, the observed optical spectrum is caused by the excitation in the organic part of the MOF film, this means in the *R*-MeBINOL-PorDC linker. In the UV/Vis spectrum in the range from approximately 400 to 600 nm, the Soret and Q bands are clearly visible. Compared to the molecules in solution, the bands in the SURMOF are red-shifted. The Soret band shifts from 421 nm to 437 nm. This is caused by the close packing of porphyrin linkers in the SURMOF and was also found in our previous work.^[17] The band at approximately 230 nm is assigned to the π - π^* excitation of the BINOL moiety.^[24] There is only a small red-shift (of only 4 nm) when comparing the band from the linker in solution and in the SURMOF. Compared to the

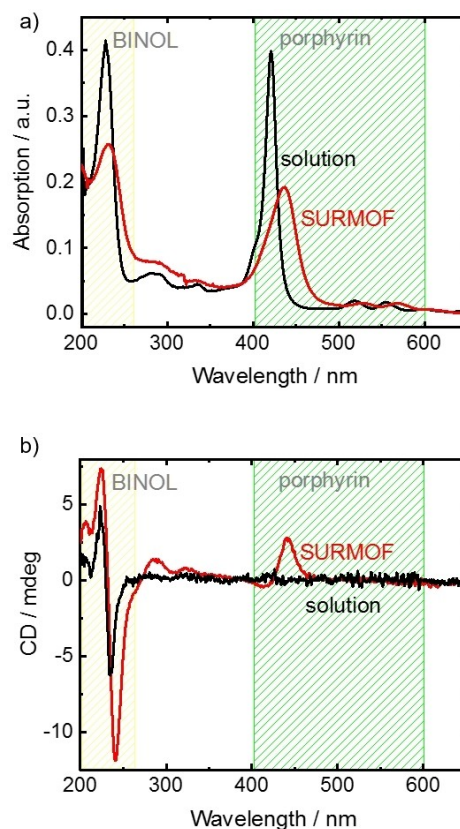


Figure 2. a) UV/Vis and b) CD spectra of the SURMOF Zn(*R*-MeBINOL-PorDC) (red) and of the *R*-MeBINOL-PorDC linker dissolved in ethanol (black). All spectra were measured in transmission mode. The region of the Soret and Q bands of porphyrin are highlighted in green. The region of the π - π^* excitation in the BINOL moiety is highlighted in yellow.

linker in solution, all absorption bands of the SURMOF are broadened.

Circular dichroism (CD) spectroscopy was performed to explore the optical activity and the chirality of the material, Figure 2b. Both, *R*-MeBINOL-PorDC in ethanol and in the SURMOF (see Figure 2b) show strong CD signals at 200–260 nm, attributed to the chiral BINOL groups.^[24] Most interestingly, while there is no significant CD band for the molecule in solution in the entire range above 260 nm, the SURMOF shows a clear CD band at 440 nm. Most likely, this CD band is caused by the Soret band of porphyrin, see UV/Vis spectra. This means, the porphyrin moiety, which is not active in solution, is optically active in the SURMOF. This indicates structural changes of the porphyrin linkers by their assembly in the SURMOF.

For additional experimental proof of the optical activity and chirality of the Zn(*R*-MeBINOL-PorDC) SURMOF, we characterized the SURMOF by diffuse reflection CD (DRCD) and fluorescence detected CD (FDCD) spectroscopy. The results are shown in Figure S2. All the data are in agreement with the CD spectra and verifies that the porphyrin-SURMOF exhibits a chiral structure. The spectrum of circularly polarized luminescence, where no clear bands were found, is shown in Figure S22.

The preparation of the same SURMOF film but without chiral BINOL-side groups results in an optically inactive, i.e. achiral, structure, Figure S17. This supports the hypothesis that the chirality in the Zn(*R*-MeBINOL-PorDC) SURMOF, meaning the structural changes causing chirality, i.e. twisting of the porphyrin core, is caused by the molecular assembly in a MOF and by the BINOL-side groups (as discussed further below).

To further understand the molecular structure as well as its structural changes caused by the assembly, detailed calculations using density functional theory (DFT) were performed, see Supporting Information. The absorption and chiroptical spectra were calculated by time-dependent DFT. The calculated UV/Vis spectrum of the optimized (isolated) *R*-MeBINOL-PorDC linker, Figure S3, shows the presence of Q- and Soret bands of the porphyrin core and the light absorption by the BINOL moieties. This is in agreement with the experimentally measured spectrum, see Figure 2. The theoretically calculated spectrum shows slight splitting of the Soret band due to the N–H protons of porphyrin, breaking its symmetry. (This is also discussed below.)

Figure 3a and Figure S5 show the optimized structure of the Zn(*R*-MeBINOL-PorDC) SURMOF. Due to the metal-organic coordination and the restricted arrangement of the linker molecules in the three-dimensional MOF scaffold, the geometry of the porphyrin core is changing by the packing: The aromatic moiety is less planar and a twist of one of the pyrrole subunits occurs. In Figure 3b, the overlap of the porphyrin core of the isolated linker (as found in solution) and of the linker extracted from the SURMOF is shown. It visualizes the main structural change of the porphyrin moiety induced by the MOF assembly. Generally, isolated *R*-MeBINOL-PorDC has an essentially planar porphyrin core. Upon the assembly of *R*-MeBINOL-PorDC in the MOF lattice, the porphyrin core is slightly twisted and less planar (Figure S7). To quantitatively describe the degree of the planarity (or non-chirality), i.e. the out-of-plane deviation of the porphyrin core, we have introduced a custom planarity measure—the planarity breach—which is the (least) sum of squared distances of the best-fit plane to the porphyrin atoms. A planarity breach coefficient of zero indicates a completely flat and achiral porphyrin ring, while values higher than zero indicate a curved molecule. The isolated *R*-MeBINOL-PorDC linker is characterized by a low planarity breach coefficient of 0.15. The small difference to a fully planar structure originates from the covalently attached BINOL groups to the porphyrin core that may impact its vibrational flexibility, causing slight changes in the frontier orbitals. This is clearly seen in Figure S8 and S9, where CD spectra of the linkers with and without BINOL side groups are depicted. On the other hand, the planarity breach coefficient of the assembled linker equals to 0.63, which is significantly higher than of the isolated linker. This indicates a strong deviation of the porphyrin core from the planar structure upon assembly.

Further inspection of the three-dimensional SURMOF structure and assembly characteristics using NCIPLOT analysis^[25] reveals the set of intermolecular noncovalent interactions (NCI) of different nature and strength between

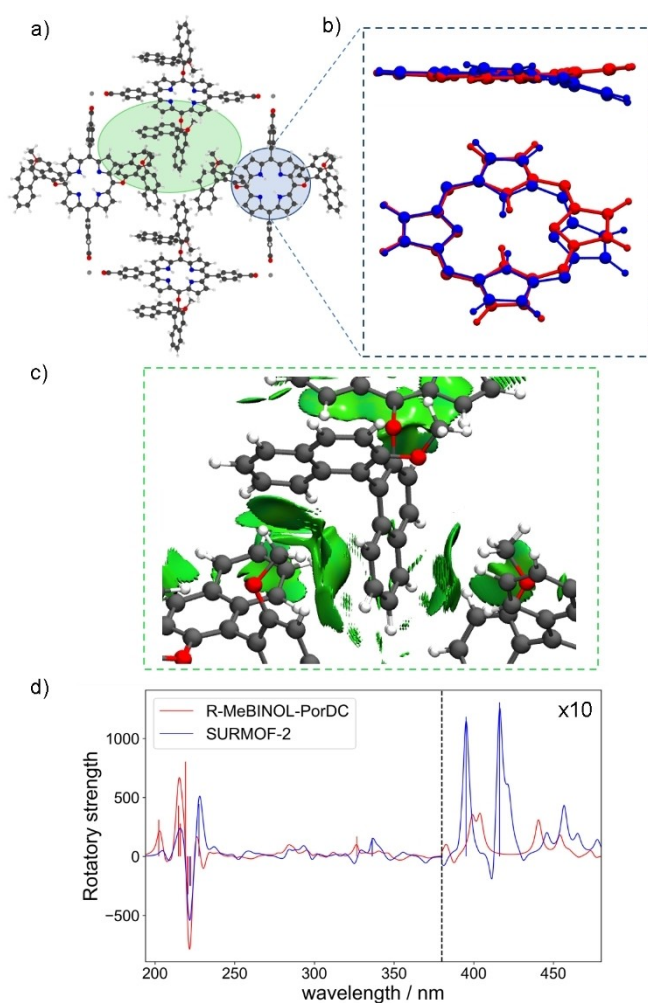


Figure 3. a) Structure of the optimized Zn(*R*-MeBINOL-PorDC) SURMOF. b) Superposition of the linker in its isolated (red) and assembled (blue) state. c) Visualization of intermolecular noncovalent interactions (areas in green) between *R*-MeBINOL-PorDC linkers assembled in the SURMOF scaffold. Intermolecular NCI surfaces correspond to the reduced density gradient of 0.4 a.u. d) Calculated CD spectra of *R*-MeBINOL-PorDC molecules in its isolated form (red) and assembled in the SURMOF (blue). Please note, the spectra above 380 nm is magnified by factor 10. Further analysis is provided in the Supporting Information.

the organic molecules in the MOF (see NCI surfaces in Figure 3c). On the one hand, hydrogen bonds and π -interactions are modulating the linker packing in the intersheet direction (see Figure S10a and S11), red-shifting the UV/Vis spectra (from 404 nm to 416 nm in the isolated form and the SURMOF, respectively, see Figure S13). On the other hand, the network of van-der-Waals (vdW), π – π and C–H \cdots π interactions between the functional BINOL side groups linked to the porphyrin (see Figure 3c, S12) triggers the SURMOF scaffold to loosen the planarity preference of the porphyrin, causing its partial twist.

The calculated CD spectra for the isolated and MOF-assembled *R*-MeBINOL-PorDC are shown in Figure 3d. The spectrum for the free linker is mainly characterized by the intense CD signal from the BINOL moiety, i.e. at

226 nm, and there is no significant chiroptical response of the porphyrin core (see Figures S4 and S14). Upon the MOF assembly, new CD signals appear at around 400 nm. These bands stem from the Soret band of the porphyrin moiety, which is permitted by the light-induced transitions between the frontier molecular orbitals, localized mostly on the aromatic porphyrin core (see Figure S6). These CD signals indicate the appearance of a chiral form of the porphyrin. In the SURMOF, the packing of the molecules and the intermolecular interactions induce the twist of one of the pyrrole rings of the porphyrin (see Figure 3b and Figure S6c,d). This twist occurs from the inherently planar form of the porphyrin moiety. The structural twist, also measured by an increase of the planarity breach coefficient (see above), is significantly higher in the Zn(*R*-MeBINOL-PorDC) SURMOF than in the isolated linker. Such structural change reduces the symmetry and modulates the electron delocalization of the highest occupied molecular orbital (HOMO), and of the HOMO-1 orbital (see Figure S6d). This reduces the symmetry. In comparison to the orbital of the isolated linker, where the electron density is equally distributed within the four pyrrole rings (Figure S6c), in the MOF, the twisted pyrrole ring has a slightly higher electron delocalization (Figure S6d). Therefore, the HOMO-1 orbital of the linker in the MOF possesses an uneven electron delocalization, i.e. asymmetry. This electron-delocalization asymmetry and the non-planar form directly contribute to the Soret band transition (i.e. its transition dipole moment) and its optical activity. This is the reason why such a chiroptical response is observed in the MOF and not observed in solution.

In addition to the twisting of the porphyrin core, the assembly in the MOF increases the energy differences between the excited state configurations of the frontier orbitals of the porphyrin, especially the energy of its HOMO orbital shown in Figure S6. It participates in the Soret band excitation to the LUMO+1 orbital, therefore, inducing the splitting of the Soret band both in UV/Vis and CD spectra (see spectra in blue in Figure 3d, S13, S14). Similar splitting has been observed in other assemblies of porphyrins^[26] and was related, among others, to the coupling between neighboring porphyrins. The electronic coupling of the HOMO and LUMO orbitals of *R*-MeBINOL-PorDC linkers in the SURMOF equals to 1.50 meV and 7.60 meV, respectively. In comparison to our previous work with a coupling between the HOMO of 6.20 meV,^[17] the coupling between HOMO orbitals decreases significantly. On the other hand, the electronic coupling between the LUMO orbitals increases approximately 30 times, i.e. from 0.27 meV to 7.60 meV. This is caused by the higher degree of charge delocalization over the whole linker, including the large BINOL groups.

Based on the excellent photophysical properties of porphyrin-SURMOFs,^[6a,17,27] we explore the photoconduction and the CPL-dissymmetry of the Zn(*R*-MeBINOL-PorDC) films. Figure 4a shows the photocurrent of the sample as response to irradiation with unpolarized light of different wavelengths, from 365 nm to 640 nm. The largest light-induced current is obtained for blue light of 455 nm. In

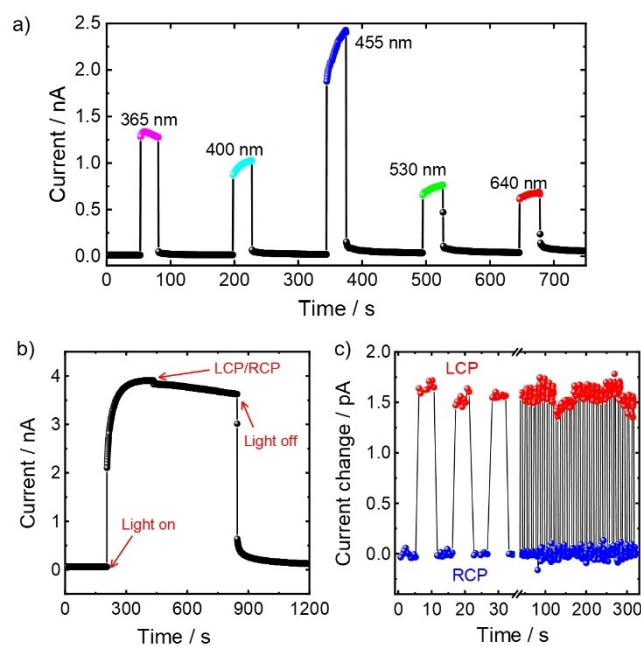


Figure 4. a) DC current versus time at a voltage of 2 V while the sample is irradiated with light of 640 nm, 530 nm, 455 nm, 400 nm and 365 nm wavelength, respectively, see labels. The base-current (in the dark) is approximately 11 pA. b) DC current versus time under 450 nm RCP and LCP illumination, see labels (and Figure S14). c) Current change when switching the light polarization every 5 seconds from RCP (blue) to LCP (red) and vice versa. This was repeated for 50 cycles. The baseline is set to the photocurrent under RCP light.

agreement with previous work,^[17] we assign this to the Soret-band excitation. Here, an On-Off-ratio of approximately 200 is realized.

The response to CPL is explored in Figure 4b and c. The sample is irradiated with light of 450 nm, where the polarization was switched from right-CPL (RCP) to left-CPL (LCP) every 5 seconds. After subtracting the baseline, Figure 4c shows the photocurrent changes between RCP and LCP. Under LCP the photocurrent is approximately 1.6 pA larger than under RCP. This corresponds to a dissymmetry factor g of 4.3×10^{-4} (with $g = 2(I_{LCP} - I_{RCP}) / (I_{LCP} + I_{RCP})$ with I denoting the photocurrent^[28]). By analyzing the CD and UV/Vis spectra, a dissymmetry of 4.7×10^{-4} is determined, which agrees well with the dissymmetry factor of the photoconduction. This supports the interpretation that the handedness-dependent CPL photoconduction is a result of the optical activity of the porphyrin.

As reference experiments, the responses to RCP and LCP irradiation of 365 nm and 625 nm are explored, Figure S16. For both wavelengths, no handedness-dependence of the CPL was recorded. The CPL data from all three wavelengths are in agreement with the CD spectra, Figure 2b, where a CD band is observed at approximately 450 nm, but not at 365 nm or 625 nm.

It should be noted that chiral porphyrin compounds and compounds of other molecules with significantly larger g -factors (for luminescence, i.e. g_{lum}) were presented.^[29]

However, the assembly of chiral materials with simultaneously strong optoelectronic and chiral properties based on porphyrin has not yet been demonstrated.

Conclusion

A chiral, crystalline porphyrin-based film is presented. The porphyrin molecules possess homochiral BINOL side groups. When the molecules are dissolved, the porphyrin core is planar and, thus, achiral. Upon assembly of the molecules in crystalline films of surface-mounted MOFs, the porphyrin core is twisted resulting in a chiral shape. DFT-based calculations show that the twisting of the porphyrin is caused by the ordered packing in the MOF and the network of noncovalent intermolecular interactions, especially between the BINOL side groups. The close packing of the porphyrin cores combined with the asymmetry of the electron density delocalization, thus, the chirality induction, allows the realization of a porphyrin-based chiral optoelectronic film for the first time. When the film is irradiated with blue light, exciting the Soret band, the film shows excellent photoconduction properties with a large On-Off-photoconduction ratio. For photoconduction with circularly polarized light, a dissymmetry factor g of 4.3×10^{-4} is determined, showing its chiral optoelectronic properties.

We foresee that the demonstrated assembly-modulated chirality induction in porphyrin can be combined with various methods of the extensive chemistry known to functionalize porphyrin. For example, the functionalization with electron-poor or electron-rich groups will allow the tuning of the excitation wavelength. Moreover, we believe similar methods to prepare chiroptical materials can be applied to similar materials based on phthalocyanine, perylene diimide and benzodithiophene.

Acknowledgements

This research was funded by the Deutsche Forschungsgemeinschaft (DFG, via SPP 1928 COORNETs and via HE 7036/5) and the China Scholarship Council (CSC). Authors acknowledge the Virtual Materials Design initiative (Virt-Mat) funded by KIT. M.K. acknowledges funding by the Ministry of Science, Research and Art of Baden-Württemberg (Germany) under Brigitte-Schlieben-Lange-Programm. Authors thank to Mr. Mersad Mostaghimi for providing the developer version of the MOF workflow. Open Access funding enabled and organized by Projekt DEAL.

Conflict of Interest

The authors declare no conflict of interest.

Data Availability Statement

The data that support the findings of this study are available from the corresponding author upon reasonable request.

Keywords: BINOL · Chiral Porphyrin · Circularly Polarized Light · Metal-Organic Frameworks · Photodetectors

- [1] a) W. Ma, L. Xu, A. F. de Moura, X. Wu, H. Kuang, C. Xu, N. A. Kotov, *Chem. Rev.* **2017**, *117*, 8041–8093; b) R. Schreiber, N. Luong, Z. Fan, A. Kuzyk, P. C. Nickels, T. Zhang, D. M. Smith, B. Yurke, W. Kuang, A. O. Govorov, T. Liedl, *Nat. Commun.* **2013**, *4*, 2948; c) E. Togan, Y. Chu, A. S. Trifonov, L. Jiang, J. Maze, L. Childress, M. V. Dutt, A. S. Sorensen, P. R. Hemmer, A. S. Zibrov, M. D. Lukin, *Nature* **2010**, *466*, 730–734; d) J. Petersen, J. Volz, A. Rauschenbeutel, *Science* **2014**, *346*, 67–71; e) D. A. Talmage, P. J. Curran, *Int. J. Remote Sens.* **1986**, *7*, 47–64; f) Y. Yang, R. C. da Costa, M. J. Fuchter, A. J. Campbell, *Nat. Photonics* **2013**, *7*, 634–638.
- [2] C. Chen, L. Gao, W. Gao, C. Ge, X. Du, Z. Li, Y. Yang, G. Niu, J. Tang, *Nat. Commun.* **2019**, *10*, 1927.
- [3] a) S. Park, S. W. Heo, W. Lee, D. Inoue, Z. Jiang, K. Yu, H. Jinno, D. Hashizume, M. Sekino, T. Yokota, K. Fukuda, K. Tajima, T. Someya, *Nature* **2018**, *561*, 516–521; b) Y. M. Sun, G. C. Welch, W. L. Leong, C. J. Takacs, G. C. Bazan, A. J. Heeger, *Nat. Mater.* **2012**, *11*, 44–48; c) T. Sekitani, H. Nakajima, H. Maeda, T. Fukushima, T. Aida, K. Hata, T. Someya, *Nat. Mater.* **2009**, *8*, 494–499; d) F. P. G. de Arquer, A. Armin, P. Meredith, E. H. Sargent, *Nat. Rev. Mater.* **2017**, *2*, 16100; e) J. A. Rogers, T. Someya, Y. G. Huang, *Science* **2010**, *327*, 1603–1607.
- [4] a) A. Dhakshinamoorthy, A. M. Asiri, H. Garcia, *Angew. Chem. Int. Ed.* **2016**, *55*, 5414–5445; *Angew. Chem.* **2016**, *128*, 5504–5535; b) S. Mathew, A. Yella, P. Gao, R. Humphry-Baker, B. F. E. Curchod, N. Ashari-Astani, I. Tavernelli, U. Rothlisberger, M. K. Nazeeruddin, M. Gratzel, *Nat. Chem.* **2014**, *6*, 242–247; c) L.-L. Li, E. W.-G. Diau, *Chem. Soc. Rev.* **2013**, *42*, 291–304; d) A. J. Esswein, D. G. Nocera, *Chem. Rev.* **2007**, *107*, 4022–4047.
- [5] A. Takai, C. P. Gros, J. M. Barbe, R. Guilard, S. Fukuzumi, *Chem. Eur. J.* **2009**, *15*, 3110–3122.
- [6] a) J. Liu, W. Zhou, J. Liu, I. Howard, G. Kilibarda, S. Schlabach, D. Coupry, M. Addicoat, S. Yoneda, Y. Tsutsui, T. Sakurai, S. Seki, Z. Wang, P. Lindemann, E. Redel, T. Heine, C. Wöll, *Angew. Chem. Int. Ed.* **2015**, *54*, 7441–7445; *Angew. Chem.* **2015**, *127*, 7549–7553; b) H. Imahori, T. Umeyama, S. Ito, *Acc. Chem. Res.* **2009**, *42*, 1809–1818; c) A. D. Schwab, D. E. Smith, B. Bond-Watts, D. E. Johnston, J. Hone, A. T. Johnson, J. C. de Paula, W. F. Smith, *Nano Lett.* **2004**, *4*, 1261–1265; d) M. Muccini, *Nat. Mater.* **2006**, *5*, 605–613.
- [7] a) E. Kolodzeiski, S. Amirjalayer, *Phys. Chem. Chem. Phys.* **2021**, *23*, 4728–4735; b) T.-G. Zhang, Y. Zhao, I. Asselberghs, A. Persoons, K. Clays, M. J. Therien, *J. Am. Chem. Soc.* **2005**, *127*, 9710–9720; c) S. Hiroto, Y. Miyake, H. Shinokubo, *Chem. Rev.* **2017**, *117*, 2910–3043.
- [8] a) J. T. Groves, P. Viski, *J. Org. Chem.* **1990**, *55*, 3628–3634; b) F. Burg, M. Gicquel, S. Breitenlechner, A. Pothig, T. Bach, *Angew. Chem. Int. Ed.* **2018**, *57*, 2953–2957; *Angew. Chem.* **2018**, *130*, 3003–3007; c) J. P. Collman, Z. Wang, A. Straumanis, M. Quelquejeu, E. Rose, *J. Am. Chem. Soc.* **1999**, *121*, 460–461.
- [9] a) Y. Tsuchiya, T. Shiraki, T. Matsumoto, K. Sugikawa, K. Sada, A. Yamano, S. Shinkai, *Chem. Eur. J.* **2012**, *18*, 456–465; b) Y. Tsuchiya, A. Yamano, T. Shiraki, K. Sada, S. Shinkai, *Chem. Lett.* **2011**, *40*, 99–101.

- [10] a) I. Goldberg, *CrystEngComm* **2008**, *10*, 637–645; b) S. Mashima, N. Ryu, Y. Kuwahara, M. Takafuji, H. Jintoku, R. Oda, H. Ihara, *Chem. Lett.* **2020**, *49*, 368–371; c) Y. Hizume, K. Tashiro, R. Charvet, Y. Yamamoto, A. Saeki, S. Seki, T. Aida, *J. Am. Chem. Soc.* **2010**, *132*, 6628–6629.
- [11] a) C. Maeda, K. Ogawa, K. Sadanaga, K. Takaishi, T. Ema, *Chem. Commun.* **2019**, *55*, 1064–1067; b) Y. Naruta, F. Tani, N. Ishihara, K. Maruyama, *J. Am. Chem. Soc.* **1991**, *113*, 6865–6872; c) A. C. Gehrold, T. Bruhn, H. Schneider, U. Radius, G. Bringmann, *Org. Lett.* **2015**, *17*, 210–213.
- [12] a) S. Kaskel, *The Chemistry of Metal-Organic Frameworks: Synthesis, Characterization, and Applications*, Wiley, Hoboken, **2016**; b) H. Furukawa, K. E. Cordova, M. O’Keeffe, O. M. Yaghi, *Science* **2013**, *341*, 1230444.
- [13] J. Caro, *Chem. Ing. Tech.* **2018**, *90*, 1759–1768.
- [14] a) C. G. Silva, A. Corma, H. Garcia, *J. Mater. Chem.* **2010**, *20*, 3141–3156; b) A. A. Talin, A. Centrone, A. C. Ford, M. E. Foster, V. Stavila, P. Haney, R. A. Kinney, V. Szalai, F. El Gabaly, H. P. Yoon, F. Leonard, M. D. Allendorf, *Science* **2014**, *343*, 66–69; c) A. Dragässer, O. Shekhah, O. Zybalyo, C. Shen, M. Buck, C. Wöll, D. Schlettwein, *Chem. Commun.* **2012**, *48*, 663–665; d) L. M. Montañez, K. Müller, L. Heinke, H. J. Osten, *Microporous Mesoporous Mater.* **2018**, *265*, 185–188; e) R. Haldar, L. Heinke, C. Wöll, *Adv. Mater.* **2020**, *32*, 1905227; f) I. Stassen, N. C. Burtch, A. A. Talin, P. Falcaro, M. D. Allendorf, R. Ameloot, *Chem. Soc. Rev.* **2017**, *46*, 3853–3853; g) P. Falcaro, R. Ricco, C. M. Doherty, K. Liang, A. J. Hill, M. J. Styles, *Chem. Soc. Rev.* **2014**, *43*, 5513–5560; h) “Dyes and Photoactive Molecules in Microporous Systems”: H. A. Schwartz, U. Ruschewitz in *Structure and Bonding, Vol. 183* (Eds.: V. Martinez Martinez, F. L. Arbeloa), Springer, Berlin, **2020**, pp. 105–153.
- [15] a) O. Shekhah, H. Wang, S. Kowarik, F. Schreiber, M. Paulus, M. Tolan, C. Sternemann, F. Evers, D. Zacher, R. A. Fischer, C. Wöll, *J. Am. Chem. Soc.* **2007**, *129*, 15118–15119; b) L. Heinke, C. Wöll, *Adv. Mater.* **2019**, *31*, 1806324.
- [16] a) S. Okur, P. Qin, A. Chandresh, C. Li, Z. Zhang, U. Lemmer, L. Heinke, *Angew. Chem. Int. Ed.* **2021**, *60*, 3566–3571; *Angew. Chem.* **2021**, *133*, 3609–3614; b) A. B. Kanj, J. Bürck, N. Vankova, C. Li, D. Mutruc, A. Chandresh, S. Hecht, T. Heine, L. Heinke, *J. Am. Chem. Soc.* **2021**, *143*, 7059–7068; c) Z.-G. Gu, J. Bürck, A. Bihlmeier, J. Liu, O. Shekhah, P. G. Weidler, C. Azucena, Z. Wang, S. Heissler, H. Gliemann, W. Klopfer, A. S. Ulrich, C. Wöll, *Chem. Eur. J.* **2014**, *20*, 9879–9882; d) M. Padmanaban, P. Muller, C. Lieder, K. Gedrich, R. Grunker, V. Bon, I. Senkovska, S. Baumgartner, S. Opelt, S. Paasch, E. Brunner, F. Glorius, E. Klemm, S. Kaskel, *Chem. Commun.* **2011**, *47*, 12089–12091.
- [17] X. Liu, M. Kozłowska, T. Okkali, D. Wagner, T. Higashino, G. Brenner-Weiß, S. M. Marschner, Z. Fu, Q. Zhang, H. Imahori, S. Bräse, W. Wenzel, C. Wöll, L. Heinke, *Angew. Chem. Int. Ed.* **2019**, *58*, 9590–9595; *Angew. Chem.* **2019**, *131*, 9691–9696.
- [18] a) C. Zhang, X. Wang, L. Qiu, *Front. Chem.* **2021**, *9*, 711488; b) P. C. Mondal, D. Asthana, R. K. Parashar, S. Jadhav, *Mater. Adv.* **2021**, *2*, 7620–7637; c) X. Shang, I. Song, J. H. Lee, M. Han, J. C. Kim, H. Ohtsu, J. Ahn, S. K. Kwak, J. H. Oh, *J. Mater. Chem. C* **2019**, *7*, 8688–8697.
- [19] R. Haldar, C. Wöll, *Nano Res.* **2021**, *14*, 355–368.
- [20] A. Chandresh, X. Liu, C. Woell, L. Heinke, *Adv. Sci.* **2021**, *8*, 2001884.
- [21] J. X. Liu, B. Lukose, O. Shekhah, H. K. Arslan, P. Weidler, H. Gliemann, S. Bräse, S. Grosjean, A. Godt, X. L. Feng, K. Mullen, I. B. Magdau, T. Heine, C. Wöll, *Sci. Rep.* **2012**, *2*, 921.
- [22] Deposition Number 2225175 contains the supplementary crystallographic data for this paper. These data are provided free of charge by the joint Cambridge Crystallographic Data Centre and Fachinformationszentrum Karlsruhe Access Structures service. Since no single-crystal XRD data are available, the structure is based on the out-of-plane XRD and DFT data.
- [23] W. Zhou, S. Begum, Z. Wang, P. Krolla, D. Wagner, S. Braese, C. Wöll, M. Tsotsalas, *ACS Appl. Mater. Interfaces* **2018**, *10*, 1528–1533.
- [24] N. Berova, L. Di Bari, G. Pescitelli, *Chem. Soc. Rev.* **2007**, *36*, 914–931.
- [25] a) J. Contreras-García, W. Yang, E. R. Johnson, *J. Phys. Chem. A* **2011**, *115*, 12983–12990; b) E. R. Johnson, S. Keinan, P. Mori-Sánchez, J. Contreras-García, A. J. Cohen, W. Yang, *J. Am. Chem. Soc.* **2010**, *132*, 6498–6506.
- [26] a) L. Zanetti-Polzi, A. Amadei, R. Djemili, S. Durot, L. Schoepff, V. Heitz, B. Ventura, I. Daidone, *J. Phys. Chem. C* **2019**, *123*, 13094–13103; b) Y. Matano, K. Matsumoto, Y. Terasaka, H. Hotta, Y. Araki, O. Ito, M. Shiro, T. Sasamori, N. Tokitoh, H. Imahori, *Chem. Eur. J.* **2007**, *13*, 891–901; c) G. de Miguel, K. Hosomizu, T. Umeyama, Y. Matano, H. Imahori, M. T. Martin-Romero, L. Camacho, *ChemPhysChem* **2008**, *9*, 1511–1513; d) F. Koch, M. Kullmann, U. Selig, P. Nuernberger, D. C. G. Götz, G. Bringmann, T. Brixner, *New J. Phys.* **2013**, *15*, 025006.
- [27] J. X. Liu, W. C. Zhou, J. X. Liu, Y. Fujimori, T. Higashino, H. Imahori, X. Jiang, J. J. Zhao, T. Sakurai, Y. Hattori, W. Matsuda, S. Seki, S. K. Garlapati, S. Dasgupta, E. Redel, L. C. Sunag, C. Woll, *J. Mater. Chem. A* **2016**, *4*, 12739–12747.
- [28] P. Stachelek, L. MacKenzie, D. Parker, R. Pal, *Nat. Commun.* **2022**, *13*, 553.
- [29] a) C. Maeda, K. Ogawa, K. Sadanaga, K. Takaishi, T. Ema, *Chem. Commun.* **2019**, *55*, 1064–1067; b) J.-R. Jiménez, M. Poncet, S. Míguez-Lago, S. Grass, J. Lacour, C. Besnard, J. M. Cuerva, A. G. Campaña, C. Piguet, *Angew. Chem. Int. Ed.* **2021**, *60*, 10095–10102; *Angew. Chem.* **2021**, *133*, 10183–10190; c) Y. Wu, C. Yan, X.-S. Li, L. H. You, Z.-Q. Yu, X. Wu, Z. Zheng, G. Liu, Z. Guo, H. Tian, W.-H. Zhu, *Angew. Chem. Int. Ed.* **2021**, *60*, 24549–24557; *Angew. Chem.* **2021**, *133*, 24754–24762; d) R. Q. Wang, S. B. Chen, Q. R. Chen, H. Y. Guo, F. F. Yang, *Dyes Pigm.* **2021**, *190*, 10.1016/j.dye-pig.2021.109332.

Manuscript received: November 25, 2022

Accepted manuscript online: December 14, 2022

Version of record online: ■■■, ■■■

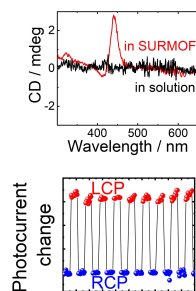
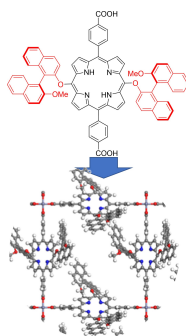
Research Articles

Metal-Organic Frameworks

C. Li, H. Schopmans, L. Langer,
S. Marschner, A. Chandresh, J. Bürck,
Y. Tsuchiya, A. Chihaya, W. Wenzel,
S. Bräse, M. Kozłowska,*

L. Heinke* e202217377

Twisting of Porphyrin by Assembly in a Metal-Organic Framework yielding Chiral Photoconducting Films for Circularly-Polarized Light Detection



By incorporating functionalized porphyrin in a crystalline lattice of a metal-organic framework thin film, the porphyrin core twists and becomes chiral. The chiral porphyrin thin film shows excellent optoelectronic properties with different photocurrents for right- and left-circularly polarized light.